Direct Dynamics Simulations of O(^{3}P) + HCl at Hyperthermal Collision Energies

Jon P. Camden and George C. Schatz*

Department of Chemistry, Northwestern University, Evanston, Illinois 60208-3113

Received: September 29, 2006; In Final Form: November 1, 2006

The dynamics of the O(^{3}P) + HCl reaction at hyperthermal collision energies were investigated using the quasiclassical trajectory method. Stationary points on the OClH $^3A''$ and $^3A'$ potential energy surfaces (PESs) were also examined. The lowest transition state leading to OCl + H on the $^3A''$ surface is 2.26 eV above the reagents at the CCSD(T)/cc-pVTZ level of theory. This saddle point is bent and product-like. Direct dynamics calculations at the MP2/cc-pVTZ level of theory were used to investigate the excitation functions for OH + Cl, OCl + H, and O + H + Cl formation. OCl is formed mainly from small-impact-parameter collisions, and the OCl + H excitation function peaks around 5 eV, where it is similar in magnitude to the OH + Cl excitation function. The shape of the OCl + H excitation function is discussed, and features are identified that should be general to hyperthermal collision dynamics.

I. Introduction

The need to understand and control chemistry in extreme environments is motivating new theoretical[1] and experimental[2−4] explorations of reactions at hyperthermal collision energies. The large amount of energy available in these collisions can drive chemical transformations that are typically forbidden at thermal energies. The earliest studies of hot-atom chemistry[5] were unfortunately limited by difficult-to-define experimental conditions and a lack of accurate theoretical methods. Therefore, fundamental questions concerning product branching ratios, energy partitioning, and mechanistic details remain unanswered for these high-energy transformations. It is the goal of this work to use a model system to explore the mechanism of H-atom elimination and fragmentation in the collisions of O(^{3}P) with HCl. Indeed, we believe that this work illustrates features of H-elimination excitation functions that are general to hyperthermal reactions of the type H + HL (heavy + heavy−light).

Recent simulations by Levin and co-workers[6] have shown that hyperthermal O + HCl chemistry plays an important role in the reacting flows that result from the interaction of a jet and the rarefied atmosphere found at high altitudes. Their study illustrates the need for accurate reaction cross sections and product branching ratios at high energies. From a fundamental dynamics perspective, O(^{3}P) + HCl is a benchmark system, and increasingly sophisticated experimental and theoretical methods have been applied to its study. Although it is known that OCl can be formed by the reaction of electronically excited O(^{1}D) with HCl,[7] studies employing O(^{3}P)[8−12] have looked exclusively at the OH + Cl product channel.

Over the years, several potential energy surfaces (PESs) for the lowest ($^3A''$) and first excited ($^3A'$) triplet states of the OHCl system have been constructed. We note that the $^3A''$ and $^3A'$ surfaces are degenerate for collinear geometries. The early LEPS surfaces[13] predicted a linear transition state for OH + Cl formation (TS1); however, the first $^3A''$ surface to correctly describe the bent transition character of this transition state was proposed by Koizumi, Schatz, and Gordon (KSG).[9] The KSG surface was based on scaled ab initio points at the MP2/6-31G-(d,p) level of theory. A new ($^3A''$) surface based on scaled MRCI+Q/cc-pVTZ energies was reported by Ramachandran, Schrader, Senekowitsch, and Wyatt[10] in 1999. Ramachandran and Peterson[11] (RP) in 2003 used high-level electronic structure calculations to characterize various stationary points on the OClH PES, such as reagents, products, van der Waals complexes, and the lowest-lying transition state, which leads to OH + Cl products. Points calculated at the MRCI+Q/CBS level were then used to construct new $^3A''$ and $^3A'$ PESs. However, the RP surface is limited to studies of total energy less than 1.73 eV and is unsuited to the work presented here. In fact, none of the previous surfaces have been calibrated for the formation of OCl. Given the unavailability of a global PES that is capable of treating both OCl product formation and high-energy collisions (3−7 eV), we utilized direct dynamics calculations. In this method, the energies and gradients are calculated "on-the-fly" as the trajectory is propagated, which avoids the costly development of a global PES and allows for easy extension of the method to other reactions with more degrees of freedom.

II. Theoretical Methods

A. Stationary Point Characterization. In this section, we seek to characterize the lowest-lying transition state leading to OCl + H on the $^3A''$ PES (TS2) at a high level of theory and to explore lower-level methods computationally tractable for direct dynamics simulations. Further, we make a limited investigation of TS2 on the $^3A'$ surface to assess its possible contribution to the OCl + H reaction cross section. Calculations of the saddle points were performed with the Q-Chem version 2.1[14] and GAMESS[15] electronic structure codes, and the results are compiled in Tables 1 and 2. Coupled-cluster calculations with singles, doubles, and perturbative triples[16] [CCSD(T)] employing the cc-pVTZ basis set and frozen-core approximation represent the highest level of theory employed on $^3A''$. At this level, we find that the $^3A''$ transition state leading to OCl + H is bent ($\theta_{OClH} = 158.0$) and product-like ($r_{OCl} = 1.63$ Å and $r_{HCl} = 1.88$ Å). This is consistent with Hammond's postulate,

* To whom correspondence should be addressed. E-mail: schatz@chem.northwestern.edu.

10.1021/jp0664162 CCC: $33.50
Published on Web 12/21/2006

TABLE 1: Energetics and Transition-state Properties for the O + HCl → OH + Cl, O + HCl → OCl + H, and O + HCl → O + H + Cl Reactions on the $^3A''$ Surface[a]

	UMP2/6-31G(d,p)	UMP2/cc-pVTZ	B3LYP/6-31G(d,p)[b]	CCSD(T)[c]	expt[d]
		O + HCl → TS1 → OH + Cl			
ΔE	0.026 (0.072)	0.057 (0.104)	−0.089 (-0.044)	0.045 (0.091)	(0.022)
$\Delta E^{\ddagger}$	0.817 (0.730)	0.695 (0.610)	0.024(-0.045)	0.482[e]	
r_{HCl}	1.44	1.44	1.40	1.44[e]	
r_{OH}	1.20	1.20	1.34	1.23[e]	
θ_{OHCl}	135.1	135.6	136.5	135.1[e]	
		O + HCl → TS2 → OCl + H			
ΔE	2.209 (2.069)	2.107 (1.970)	1.875 (1.740)	2.096 (1.961)	(1.683)
$\Delta E^{\ddagger}$	2.737 (2.626)	2.461(2.353)	1.894 (1.766)	2.264 (2.144)	
r_{OCl}	1.66	1.60	1.64	1.63	
r_{HCl}	1.71	1.71	2.09	1.88	
θ_{OClH}	156.6	158.0	156.9	158.0	
		O + HCl → O + H + Cl			
ΔE	4.212 (4.018)	4.524 (4.335)	4.471 (4.285)	4.506 (4.320)	(4.432)

[a] Energies in electronvolts and distances in angstroms. Harmonic zero-point-corrected values for reaction energies and barrier heights are in parentheses. [b] Larger-basis-set DFT calculations using the B3LYP functional can be found in ref. 19. [c] UCCSD(T)/cc-pVTZ calculations from this work. [d] D_0(HCl) = 102.2 kcal/mol and D_0(OCl) = 63.4 kcal/mol from ref 25; revised value of D_0(OH) = 101.76 from ref 26. Values include spin−orbit effects, whereas our calculations do not. [e] R/UCCSD(T)/AVQZ′+d calculations from ref 11.

TABLE 2: Properties of the Transition States Leading to OCl + H Formation on the $^3A''$ and $^3A'$ Surfaces at the ROHF-MP2/cc-VTZ Level of Theory.[a]

	$^3A'$	$^3A''$
$\Delta V^{\ddagger}$	2.441	2.472
r_{O-Cl}	1.62	1.65
r_{H-Cl}	1.74	1.70
θ_{OHCl}	160.1	180.0
frequencies	1745i	1485i
	421	337
	680	707

[a] Energies in electronvolts and distances in angstroms.

which states that, for endothermic reactions, the transition state is late, i.e., product-like.

To characterize TS2 on the $^3A'$ surface, we employed ROHF-MP2/cc-pVTZ calculations, the results of which are reported in Table 2. A method based on a restricted open-shell reference wave function was chosen so that the desired symmetry could be obtained by systematically reordering the molecular orbitals in GAMESS. We were careful to examine the interchange of several occupied and unoccupied orbitals to ensure that the first excited state of $^3A'$ symmetry was found. We also include calculations of TS2 at the ROHF-MP2/cc-pVTZ level on the $^3A''$ surface in Table 2 for comparison with those in Table 1, which were obtained with UHF wavefunctions. We find that TS2 is linear on the $^3A'$ surface, analogous to the linear transition state leading to OH + Cl (TS1) found by Ramachandran and Peterson[11] on the $^3A'$ surface. Although calculations of the reaction cross sections on $^3A'$ are beyond the scope of this work, we did examine the shape of the potential energy surface around TS2 to assess its possible contribution to the dynamics. Figure 1 shows a plot the potential energy as a function of the O−H−Cl bending angle (θ_{O-Cl-H}) with the bond lengths frozen at their transition-state values for the respective $^3A''$ and $^3A'$ surfaces. It is clear that TS2 on $^3A'$, although quite similar in energy to TS2 on $^3A''$, has a much smaller cone of acceptance. Therefore, we can expect a small contribution to the cross section from $^3A'$ for the lower end of the energy range studied here. For example, investigations of the OH + Cl channel by Xie et al.[12] indicate a small contribution from $^3A'$ over the range of energies they studied, which is likely due to a smaller cone of acceptance for TS1 on $^3A'$ when compared to TS1 on the $^3A''$.[11] In the future, it would, of course, be desirable to quantify the contribution from $^3A'$ with dynamics calculations on a benchmark surface.

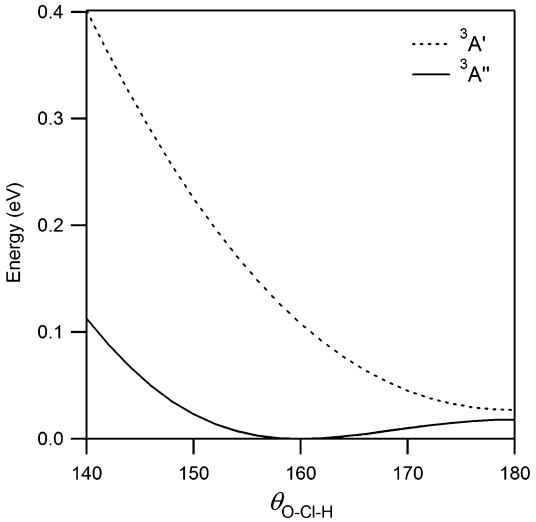

Figure 1. Potential energy as a function of O−Cl−H bending angle on the $^3A''$ and $^3A'$ surfaces. The bond lengths were frozen at their respective transition-state values for each surface and are quite similar (Table 2). The zero in energy was taken to be at the transition state leading to OCl + H on the $^3A''$ surface.

Several different combinations of basis set and electronic structure method were examined for possible use in our direct dynamics trajectories. The reaction energetics and transition-state properties calculated at the UMP2/6-31G(d,p), UMP2/cc-pVTZ, B3LYP[17,18]/6-31G(d,p), and CCSD(T)/cc-pVTZ levels are included in Table 1. B3LYP/6-31G(d,p) calculations exhibited an unacceptably small barrier to the OH + Cl channel: 0.024 eV compared to best estimate from Ramachandran and Peterson of 0.460 eV. Larger-basis-set calculations reported elsewhere[19] do not improve on this state of affairs. B3LYP also underestimates [by ∼0.4 eV compared to CCSD(T)] the barrier to OCl + H formation and shows additional transition states that are not present at higher levels of theory.[11] UMP2/6-31G(d,p), on the other hand, has a barrier that is too large for both TS1 and TS2 compared to CCSD(T); however, when a larger basis set is used, the agreement is improved. Of the computationally tractable methods examined, UMP2/cc-pVTZ shows the best agreement with the higher-level CCSD(T)/cc-pVTZ calculations and thus was used in our dynamics simulations. Indeed,

for the OCl channel, which is of primary interest here, the difference between TS2 for CCSD(T)/cc-pVTZ and MP2/cc-pVTZ is about 0.22 eV, which is only 4% of the available energy at $E_{coll} = 5$ eV.

B. Details of the Quasiclassical Trajectory Calculations. Batches of 60−250 quasiclassical trajectory calculations were run at a variety of collision energies (E_{coll}) between 3 and 7 eV to calculate reaction cross sections for the OCl + H (σ_{OCl}), OH + Cl (σ_{OH}), and O + H + Cl (σ_{frag}) product channels. The number of trajectories at each energy was chosen to obtain good statistics for the dynamical quantities of interest. Trajectories are integrated by a standard fifth-order predictor, sixth-order corrector integration algorithm.[20] At each point along the trajectory, the energy gradient was obtained from a UMP2/cc-pVTZ calculation in Q-Chem. The initial conditions were sampled randomly over initial orientations, and the HCl diatom vibrational phase was sampled from a classical harmonic oscillator distribution. The maximum impact parameter (b_{max}) ranged from 3.0 to 5.0 au, with the smaller value employed for calculations that focused only on the OCl channel ($E_{coll} = 4$, 6, and 6.5 eV). The integration time step was held constant at 10.5 au for all trajectories. Energy conservation was required to be better than 0.09 eV, which, for this system, represents a deviation of less than 1×10^{-5} of the total energy. When energy conservation violations were observed, it was due to problems in convergence of the self-consistent field (SCF) calculation and not the integration time step, i.e., occasionally, the SCF calculation would fail to converge, or it would converge to the wrong state. We also checked spin contamination at each point in the integration. At the lowest collision energy, the value of $<S^2>_{max}$ was less than 2.1 for all trajectories. However, for $E_{coll} = 7$ eV, larger values of $<S^2>_{max}$ (2.5−3.0) were observed for the trajectories leading to fragmentation. However, this is to be expected when all bonds in the system are broken, and we retained these trajectories in the cross-section calculations. Integration was terminated when the distance between any two atoms exceeded 10 au. We did not discard product trajectories with an internal energy below the harmonic zero point, as this can lead to an underestimation of the cross section.[21,22] When fragmentation occurs, the light H atom can often move beyond the 10-au limit before OCl can separate; in these cases, the fragmentation into O + Cl + H is determined by energy conservation, i.e., the calculated internal energy of the OCl fragment exceeds its dissociation energy.

III. Results and Discussion

A. O(^{3}P) + HCl → OH + Cl. Figure 2a compares the reaction cross sections for OH formation (σ_{OH}) on the $^3A''$ surface calculated in this work to those of Xie et al.[12] Over the studied range (3−7 eV), we find that the cross section increases in contrast to the previous calculations. Although the PES used in the study of Xie et al. is expected to be significantly more accurate for total energies less than 1.73 eV, it has not been calibrated for the high energy range reported here. It is worth noting that our MP2/cc-pVTZ direct dynamics simulations converge toward the Xie et al. cross sections at the lower end of our energy range. Thus, it is likely that our direct dynamics calculations are capturing the essential details over the studied energy range of this work.

The amount of energy partitioned into the relative translation of the OH + Cl pair as a fraction of the total energy available to the products ($f_{T',OH+Cl}$) is reported in Table 3, along with the average value of the scattering angle ($<\cos\theta>$). The reagent translational energy is mostly partitioned into product translation,

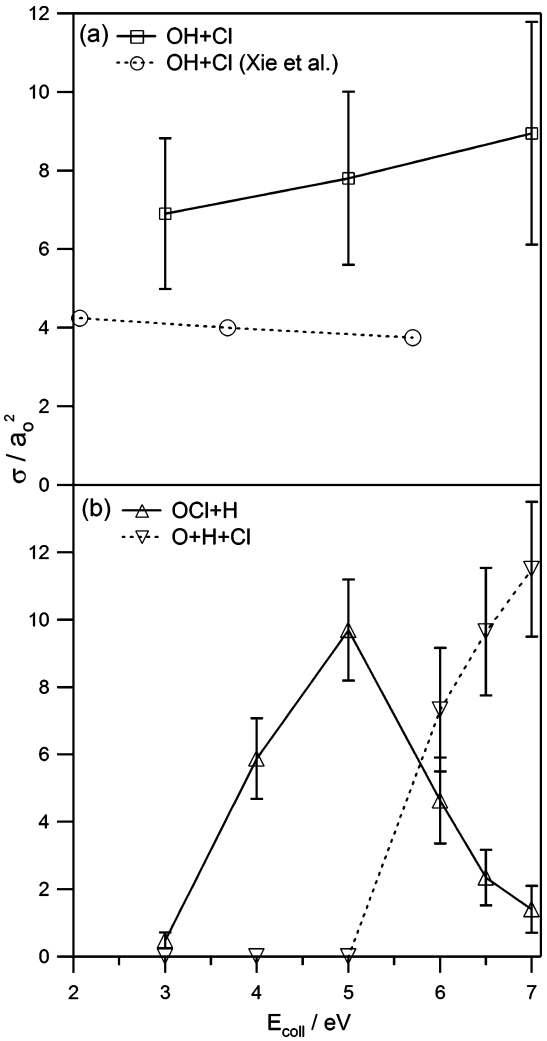

Figure 2. Calculated reaction cross sections for the reaction of O(^{3}P) + HCl on the $^3A''$ surface obtained from the quasiclassical trajectory method at the UMP2/cc-pVTZ level of theory. (a) Cross section for the OH + Cl product channel (□) compared to ref 12 (○). (b) Cross sections for the OCl + H (△) and O + H + Cl (▽) product channels. The statistical uncertainty results from the number of trajectories (N) in each bin and is given by $\sqrt{N}/N$.

TABLE 3: Product Energy Disposal and Average Scattering Angle of the Molecular Product with Respect to the Incident O Atom Velocity.

E_{coll} (eV)	$f_{T,OH+Cl}$[a]	$f_{T,OCl+H}$[a]	$<\cos\theta>_{OH+Cl}$	$<\cos\theta>_{OCl+H}$
3	0.67	−[b]	0.27	−
5	0.70	0.45	0.46	−0.34
7	0.74	−	0.78	−

[a] Value listed is the relative translational energy of the products as a fraction of the total energy available to the products. [b] The small number of trajectories that produce OCl + H at $E_{coll} = 3$ and 7 eV leads to a large statistical uncertainty in the energy partitioning and average scattering angle.

and the fraction remains constant over the studied range. The opacity function plotted in Figure 3a shows that OH + Cl formation favors larger impact parameters. The OH product scatters into the forward hemisphere with respect to the incident O-atom velocity, as illustrated by the differential cross section in Figure 3b. At the highest collision energies, $<\cos\theta> = 0.78$ (Table 3), which indicates that a stripping mechanism dominates. The favoring of larger impact parameters, the forward scattering of the OH product, and the large fraction of energy in product

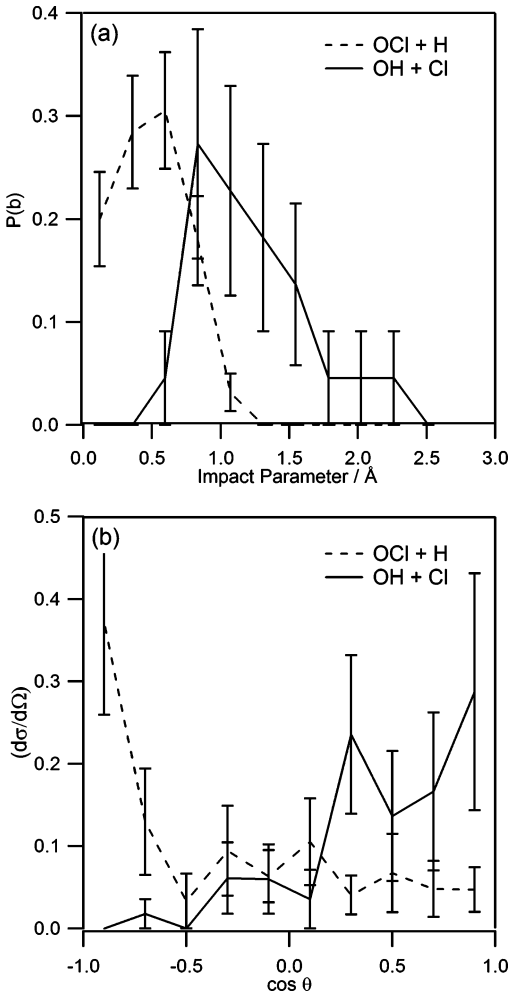

Figure 3. (a) Opacity functions and (b) differential cross sections (DCSs) for the OH + Cl (solid line) and OCl + H (dashed line) product channels for $E_{coll} = 5$ eV. Forward scattering is defined with respect to the incident O-atom velocity vector, and in each case, the DCS of the molecular product is given. All curves are normalized such that the area under each is 1. The statistical uncertainty results from the number of trajectories (N) in each bin and is given by $\sqrt{N}/N$.

translation is typical for a reaction of the type H + LH → HL + H at high energies, and it is not discussed further.

B. $O(^3P) + HCl \rightarrow OCl + H$ and $O(^3P) + HCl \rightarrow O + Cl + H$. The calculated reaction cross sections for OCl + H, OH + Cl, and fragmentation are displayed in Figure 1b. OCl formation is energetically allowed at the MP2/cc-pVTZ level for $E_{coll} > 1.97$ eV, and fragmentation can occur for $E_{coll} > 4.34$ eV. σ_{OH} increases slowly over the given range, whereas fragmentation is important only at the highest energies. After the barrier (1.97 eV) to OCl formation is surmounted, σ_{OCl} increases to a maximum around 5 eV. Concomitant with the decrease in σ_{OCl}, we see an increase in σ_{frag}; indeed, we will show that many of the fragmentation trajectories can be viewed as failed OCl reactive trajectories.

σ_{OCl} is similar in magnitude to σ_{OH} only for a portion of the studied collision energy range. Close to the threshold, σ_{OCl} is much smaller than σ_{OH}, but for values around $E_{coll} = 5$ eV, OCl is a more likely product than OH. Unlike OH formation, OCl formation favors small impact parameters and backward scattering of the molecular product, as illustrated in Figure 3a and b, respectively. We now seek to explain the general shape of the OCl excitation function and provide a basis to understand similar H-elimination reactions.

C. Discussion of the OCl + H Excitation Function. The OCl excitation function from threshold to its maximum around 5 eV is readily understood. Because the barrier is late, the effective reactive threshold is well above the energetic threshold. The large size of σ_{OCl} arises because the large chlorine atom provides a significant target even though only small impact parameters are involved. It is interesting to compare these results with those of Troya, Pascual, and Schatz, who studied the $O(^3P)+CH_4 \rightarrow OCH_3+H$ reaction at collision energies up to 5 eV.[23] They found that, as for O + HCl, the H-elimination cross section also rises quickly above 3 eV, becoming larger than that for abstraction at 4 eV. However, the cross section for H elimination in O + CH_4 is only about one-half that observed for O + HCl in this work, presumably because of the larger Cl atom. Troya et al. did not study energies above 5 eV, so we cannot make a comparison of fragmentation cross sections.

To understand the decrease in cross section around $E_{coll} = 5$ eV, we begin by examining the fraction of available energy partitioned into the relative translation of the products listed in Table 3. Here, we see that $f_{T',OH+Cl}$ stays relatively constant at about 0.7, whereas $f_{T',OCl+H}$ is much smaller, about 0.45 at 5 eV, indicating that trajectories forming OCl are more effective in converting the incident translational energy into internal energy of OCl. Further, the H-atom kinetic energy in the center-of-mass frame, averaged over trajectories leading to OCl + H or O + H + Cl, is 1.51 eV for $E_{coll} = 5$ eV and 1.87 eV for $E_{coll} = 7$ eV. Thus, the kinetic energy of the departing H atom is only weakly coupled to the reagent translational energy. As mentioned earlier, our trajectories indicate that OCl is formed mainly by low-impact-parameter collisions of the O atom with the Cl atom where the O−Cl−H angle is large, followed by ejection of the H atom from the other side. In this mechanism, the departing kinetic energy of the H atom is found to be limited, so trajectories of this type lead to fragmentation for energies larger than the sum of the O + H + Cl threshold (4.34 eV) and the average H-atom kinetic energy (1.8 eV) or roughly 6 eV. Therefore, fragmentation at the energies explored in this work can be understood as failed OCl reactions. Of course, at larger collision energies, direct cleavage of the HCl bond should be possible, but this is observed infrequently here.

We also calculate the internuclear distances r_{OCl}, r_{OH}, and r_{HCl} at the point along the trajectory where the potential energy is maximized (V_{max}). At a collision energy of 5 eV, we find that the average values are $r_{OCl,Vmax} = 1.60$, $r_{OH,Vmax} = 2.87$, $r_{HCl,Vmax} = 2.29$ Å; at $E_{coll} = 7$ eV, we find $r_{OCl,Vmax} = 1.46$, $r_{OH,Vmax} = 1.45$, and $r_{HCl,Vmax} = 1.92$ Å, again for trajectories leading to OCl + H. These values combined with the animation of representative trajectories suggest an analysis in the spirit of the Direct Interaction with Product Release (DIPR) model[24] in which the incoming O atom bonds with the Cl atom to make OCl and the H atom finds itself on a repulsive potential energy surface. The light H atom is quickly ejected before the OCl bond length changes. Figure 4 displays several cuts of the $^3A''$ PES for fixed OCl bond lengths calculated at the MP2/cc-pVTZ level. For r_{OCl} bond lengths less than the isolated OCl equilibrium bond length of 1.57 Å, the H atom experiences a repulsive force. However, this repulsion is relatively independent of the OCl bond length, as can be inferred from the two different contours plotted in Figure 4. Thus, for the dominant mechanism where O attacks the Cl atom, increasing the collision energy might compress the OCl bond, but that compression does not increase the kinetic energy imparted to the ejected H atom. Last, we note that only a rare ($\sigma_{OCl+H} < 1$ Å^2 compared to $\sigma_{frag} > 10$ Å^2) type of encounter for $E_{coll} = 7$ eV can deposit enough energy

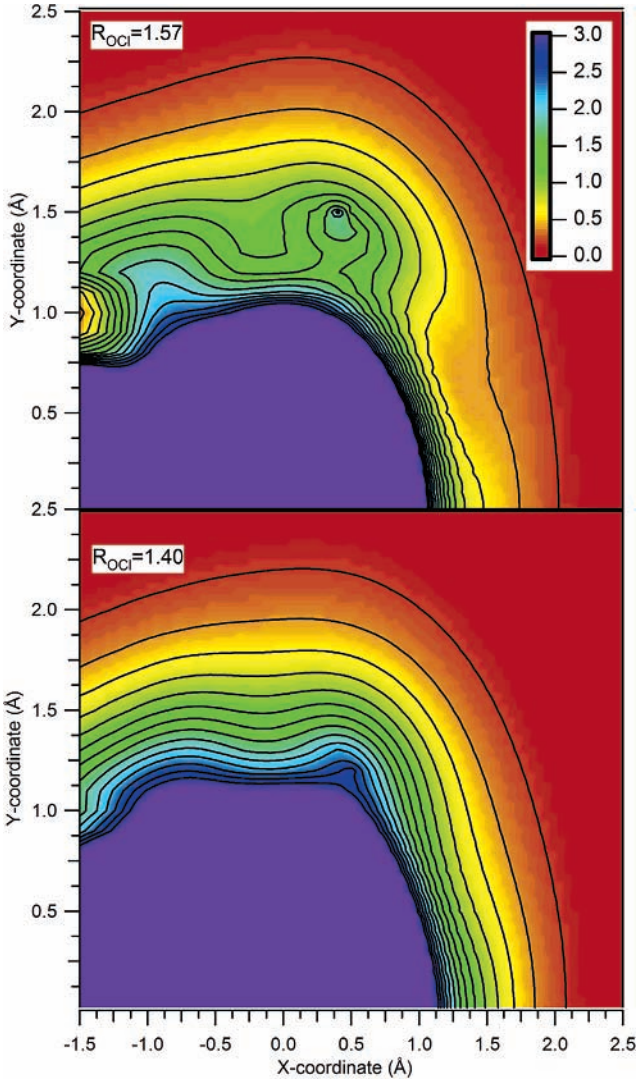

Figure 4. Contour plots of the $^3A''$ potential energy surface in electronvolts for fixed OCl bond length: (top) 1.57 Å and (bottom) 1.40 Å. The OCl bond is fixed to the *X* axis, and the Cl atom coordinate is (0.0, 0.0). The zero of each plot is taken to be when the H atom is infinitely far away.

into the relative translation of H and OCl to avoid OCl fragmentation. Examination of these trajectories reveals that OCl formation at high energy requires that the O−Cl−H angle be small (<90°). In this case, the H atom experiences a repulsion from both the Cl and O atoms, enabling it to carry away more kinetic energy. This is the only mechanism that leads to OCl formation at $E_{coll} = 7$ eV.

We therefore conclude that, if the O−Cl distance is short enough for the pair to experience a bonding interaction, the H atom will be eliminated with a kinetic energy that is determined by the repulsion of the H atom and the OCl molecule and mostly independent of the collision energy. This behavior occurs because the two heavy atoms (O and Cl) can be considered as stationary during the time when the eliminated atom (H) is in the interaction region. Further, we expect the above features to apply quite generally, extending to other H-elimination reactions. Indeed, the earlier work on O + CH_4 and our preliminary work on the O + H_2O reaction show that the H-elimination excitation function has the same shape as that observed for OCl in this work.

IV. Summary

We present new quasiclassical trajectory calculations for the collision of hyperthermal oxygen with hydrogen chloride. The cross section for OH + Cl formation slowly increases over the 3−7 eV collision energy range. The OCl + H cross section is significant only for a small window of energies, and fragmentation becomes important at the highest energies. The dominant mechanisms for each reaction channel have been identified, and the sudden decrease in OCl is discussed in terms of the maximum kinetic energy available to the OCl + H product pair. It is likely that this behavior is general and extends to other hyperthermal reactions that eliminate light atoms.

Acknowledgment. This work was supported by AFOSR and by MURI Grant F49620-01-1-0335. We thank D. Levin and T. Minton for valuable comments. J.P.C. thanks Sina Yeganeh and Christine Aikens for a critical reading of the manuscript.

References and Notes

(1) Troya, D.; Schatz, G. C. *Int. Rev. Phys. Chem.* **2004**, *23*, 341.
(2) Zhang, J. M.; Upadhyaya, H. P.; Brunsvold, A. L.; Minton, T. K. *J. Phys. Chem. B* **2006**, *110*, 12500.
(3) Gibson, K. D.; Isa, N.; Sibener, S. J. *J. Phys. Chem. A* **2006**, *110*, 1469.
(4) Fogarty, D. P.; Kandel, S. A. *J. Chem. Phys.* **2006**, *124*, 111101.
(5) Wolfgang, R. *Annu. Rev. Phys. Chem.* **1965**, *16*, 15.
(6) Gimelshein, S. F.; Levin, D. A.; Alexeenko, A. A. *J. Spacecraft Rockets* **2004**, *41*, 582.
(7) Chichinin, A. I. *Chem. Phys. Lett.* **2000**, *316*, 425.
(8) Zhang, R.; van der Zande, W. J.; Bronikowski, M. J.; Zare, R. N. *J. Chem. Phys.* **1991**, *94*, 2407.
(9) Koizumi, H.; Schatz, G. C.; Gordon, M. S. *J. Chem. Phys.* **1991**, *95*, 6421.
(10) Ramachandran, B.; Schrader, E. A., III; Senekowitsch, J.; Wyatt, R. E. *J. Chem. Phys.* **1999**, *111*, 3862.
(11) Ramachandran, B.; Peterson, K. A. *J. Chem. Phys.* **2003**, *119*, 9590.
(12) Xie, T.; Bowman, J.; Duff, J. W.; Braunstein, M.; Ramachandran, B. *J. Chem. Phys.* **2005**, *122*, 014301.
(13) Persky, A.; Broida, M. *J. Chem. Phys.* **1984**, *81*, 4352.
(14) Kong, J.; White, C. A.; Krylov, A. I.; Sherrill, C. D.; Adamson, R. D.; Furlani, T. R.; Lee, M. S.; Lee, A. M.; Gwaltney, S. R.; Adams, T. R.; Ochsenfeld, C.; Gilbert, A. T. B.; Kedziora, G. S.; Rassolov, V. A.; Maurice, D. R.; Nair, N.; Shao, Y.; Besley, N. A.; Maslen, P. E.; Dombroski, J. P.; Daschel, H.; Zhang, W.; Korambath, P. P.; Baker, J.; Byrd, E. F. C.; Van Voorhis, T.; Oumi, M.; Hirata, S.; Hsu, C.-P.; Ishikawa, N.; Florian, J.; Warshel, A.; Johnson, B. G.; Gill, P. M. W.; Head-Gordon, M.; Pople, J. A. *J. Comput. Chem.* **2000**, *21*, 1532.
(15) Schmidt, M. W.; Baldridge, K. K.; Boatz, J. A.; Elbert, S. T.; Gordon, M. S.; Jensen, J. H.; Koseki, S.; Matsunaga, N.; Nguyen, K. A.; Su, S. J.; Windus, T. L.; Dupuis, M.; Montgomery, J. A. *J. Comput. Chem.* **1993**, *14*, 1347.
(16) Raghavachari, K.; Trucks, G. W.; Pople, J. A.; Head-Gordon, M. *Chem. Phys. Lett.* **1989**, *157*, 479.
(17) Becke, A. D. *J. Chem. Phys.* **1993**, *98*, 5648.
(18) Lee, C.; Yang, W.; Parr, R. G. *Phys. Rev. B* **1988**, *37*, 785.
(19) Hsiao, C. C.; Lee, Y. P.; Want, N. S.; Wang, J. H.; Lin, M. C. *J. Phys. Chem. A* **2002**, *106*, 10231.
(20) Press, W. H.; Flannery, B. P.; Teukolsky, S. A.; Vetterling, W. T. *Numerical Recipes in FORTRAN: The Art of Scientific Computing*, 2nd ed.; Cambridge University Press: Cambridge, U.K., 1992.
(21) Kumar, S.; Sathyamurthy, N.; Ramaswamy, R. *J. Chem. Phys.* **1995**, *103*, 6021.
(22) Troya, D.; Lakin, M. J.; Schatz, G. C.; Gonzalez, M. *J. Chem. Phys.* **2001**, *115*.
(23) Troya, D.; Pascual, R. Z.; Schatz, G. C. *J. Phys. Chem. A* **2003**, *107*, 10497.
(24) Kuntz, P. J.; Mok, M. H.; Polanyi, J. C. *J. Chem. Phys.* **1969**, *50*, 4623.
(25) Huber, K. P.; Herzberg, G. *Molecular Spectra and Molecular Structure: IV. Constants of Diatomic Molecules*; Van Nostrand Reinhold: New York, 1979.
(26) Ruscic, B.; Wagner, A. F.; Harding, L. B.; Asher, R. L.; Feller, D.; Dixon, D. A.; Peterson, K. A.; Song, Y.; Qian, X. M.; Ng, C. Y.; Liu, J. B.; Chen, W. W. *J. Phys. Chem. A* **2002**, *106*, 2727.